Revista Brasileirade Física, Vol. 6, Nº 3, 1976

Calibration of the Tandem Pelletron Accelerator

V. ROTBERG, D. PEREIRA, M. N. RAO, N. UETA and O. SALA
Laboratório do Acelerador Pelletron – Departamento de Física Nuclear – Instituto de Física da Universidade de São Paulo, São Paulo SP*

Recebido em 29 de Junho de 1976

A description is given of the methods and techniques employed for the calibration of the 90° analyzing magnet coupled to the tandem Pelletron accelerator of the University of São Paulo.

É dada uma descrição dos métodos e técnicas utilizados para a calibração do imã analisador de 90° acoplado ao acelerador tandem Pelletron da Universidade de São Paulo.

1. INTRODUCTION

The installation of the University of São Paulo Pelletron accelerater' was completed in 1972. This article describes the calibration procedures for the 90° analyzing magnet* (ME-200), which defines and controls the energy of the accelerator beam (Fig.1).

As in most laboratories, the facilities at the University of São Paulo do not include a system for the absolute measurement of the beam energy, and the normal procedure is to rely on the parameters associated with the analyzing magnet itself.

---

† Postal address: Caixa Postal 20516, 01000-São Paulo SP.

* Constructed by *Varian Corporation*, U.S.A.

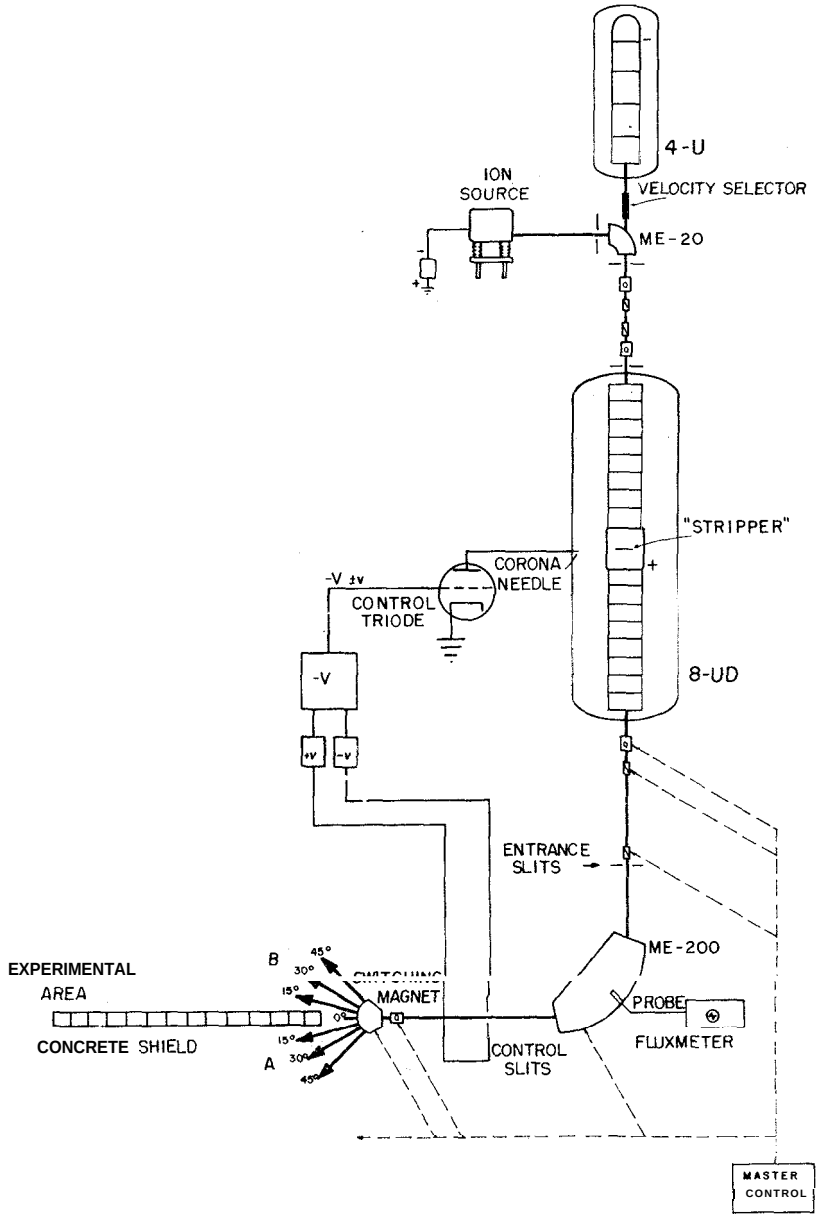

Fig.1 - Schernatics of the University of São Paulo Pelletron accelerator systern. A layout of the beam energy control system is also shown.

2. CALIBRATION PROCEDURE

The energy of an ion of mass M, charge state Z, traversing a uniform magnetic field, is given by the relativistic expression

$$E = Mc^2 \left[\left(1 + \frac{2Z^2 f^2 c^2 k}{(Mc^2)} \right)^{1/2} - 1 \right] \qquad (1)$$

where the calibration constant, k, depends essentially on the magnet geometry and type of apparatus used for measuring the magnetic field. The field strength is directly proportional to the frequency, f, of the nuclear magnetic resonance (NMR) induced in a sample of protons ($0.5 cm^3$ of water) positioned well inside the pole edges, close to the trajectory traversed by the beam.

The constant k can, in principle, be calculated for the given magnet geometry, but due to the progressive saturation of the pole pieces, a small dependence with the applied field is observed, which cannot be taken into account in the calculations. A good calibration procedure requires direct measurements of the constant k in the largest possible domain of magnet operation. This is acomplished by reproducing some strongly energy dependent feature of a nuclear reaction, such as the threshold for a (p,n) reaction, which is known to occur at a well established energy. This feature will be observed at its characteristic NMR frequency and the calibration constant can be calculated from

$$k = \frac{ME_{th}}{Z^2 f^2} \left(1 + \frac{E_{th}}{2Mc^2} \right), \qquad (2)$$

where E_{th} is its energy standard.

Neutron thresholds are favored as energy standards for calibration due to the high accuracy with which threshold energies can be measured, relative ease of reproduction and analysis of data. The observed yield of the reaction, near threshold, is proportional to $(E-E_{th})^{3/2}$ (Ref.2), and hence a plot of $(\text{yield-background})^{2/3}$ vs. energy of the beam is a straight line which intersects the energy axis at threshold.

3. ENERGY STANDARDS

A compilation of the most reliable energy standards for calibration is given by J. B. Marion[3]. However, the experience of the past decade has shown that many of these standards have to be updated in ordertoobtain the desired coherence in the resulting calibration curves. The following set was adopted in our laboratory:

a) $^{19}F(p,n)^{19}Ne$ - The energy standard is E_{th} = 4 234.3 ± .8 keV (Ref.3), an average of two independent and absolute measurements performed with magnetic spectrographs[4,5].

b) $^{12}C(\alpha,n)^{15}O$ - The value E_{th} = 11 346.3 ■ 1.7 keV (Ref.3) was based on the 1964 mass tables[6]. Recently, the mass of ^{15}O has been remeasured by Shamu *et.al.*[7] by means of the $^{15}N(p,n)^{15}O$ reaction, resulting in the new energy standard of E_{th} = 11 340.8 ± .9 keV.

c) $^{27}Al(p,n)^{27}Si$ - Marion recommends an average of two independent measurements

5 794.5 ■ 2.4 keV absolute[8] ,

5 802.9 ■ 3.8 keV relative to ThCα (Ref.9).

In spite of its relative nature, it was found that the latter value is more consistent with other standards[10,11]. This has been verified also in the present work.

d) $D(^{16}O,n)^{17}F$ - No absolute measurement of the threshold energy for this reaction exists. It can be calculated from an absolute measurement for the threshold for the $^{16}O(d,n)^{17}F$ reaction, 1 829.2 ± .6 keV (Ref.12):

$$E_{th}(^{16}O,n) = (1\ 829.2 \pm .6)\left[\frac{M_o - Q/2c^2}{M_d - Q/2c^2}\right] = 14521 \pm 5 \text{ keV},$$

where M_o, M_d are the atomic masses of oxygen and deuterium and Q is the Q-value for the $D(^{16}O,n)^{17}F$ reaction[13].

When the reaction is initiated with a particular charge state of the ^{16}O ion, the electrons attached to the nucleus will carry a significant amount of kinetic energy. Therefore, the energies defined by the magnet, at threshold, will be different for different charge states. They are calculated from

$$E_{th}(\text{magnet}) = (14\ 521 \pm 5)\left(1 - \frac{nm}{M}\right)^{-1}\ \text{keV},$$

where m is the electron mass, and n the number of electrons carried by the nucleus. The results are shown in Table I.

TABLE I

CHARGE STATE	THRESHOLD ENERGY (keV)	ELECTRON SHARE (keV)
4^+	14 523.0 ± 5	2.0
3^+	14 523.5 ± 5	2.5

4. (i) CHAMBER AND TARGETS

Figure 2 shows the scattering chamber used with solid targets. The beam enters from the right after being focused by a quadrupole lens and it is colimated by two slits placed 23cm apart. The target is positioned at left. Secondary electrons are kept in this region by the combined effect of a voltage bias and a magnetic supressor. The system is pumped by a turbo-molecular unit and pressures of the order of 10^{-7} torr were attained during experiments.

Slight modifications were introduced in order to make feasible the construction of ice targets for the $D(^{16}O,n)^{17}F$ reactions (Fig.3). A needle valve was installed, through which a small quantity of heavy water (D_2O) is introduced in the chamber and vaporized in a heated metallic surface. The vapor is allowed to diffuse throughout the chamber while the pumping speed is reduced by partially closing the valve which connects the

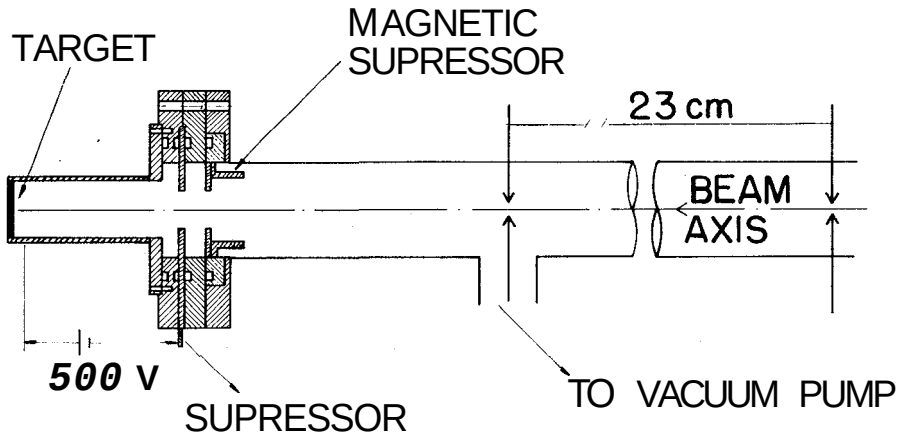

Fig.2 - Scattering chamber used for rneasuring the neutron yield frorn solid targets.

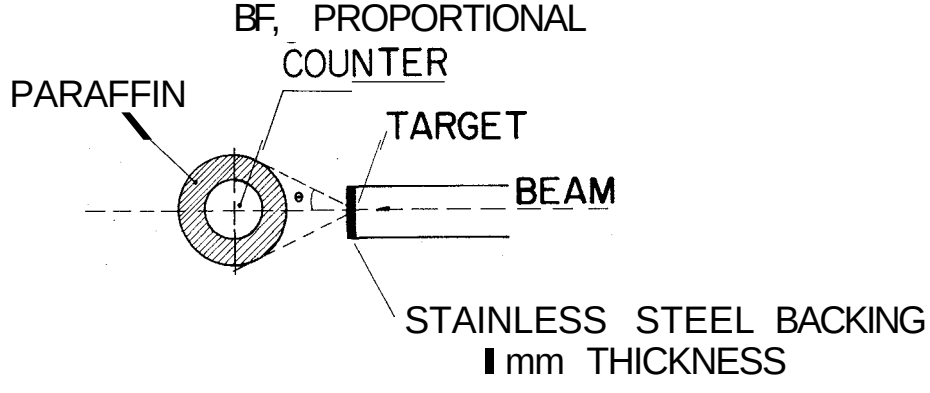

Fig.4 - Top view of slow neutron counter. The paraffin moderator defines the maximum energy above threshold useful for the search of the threshold frequencies.

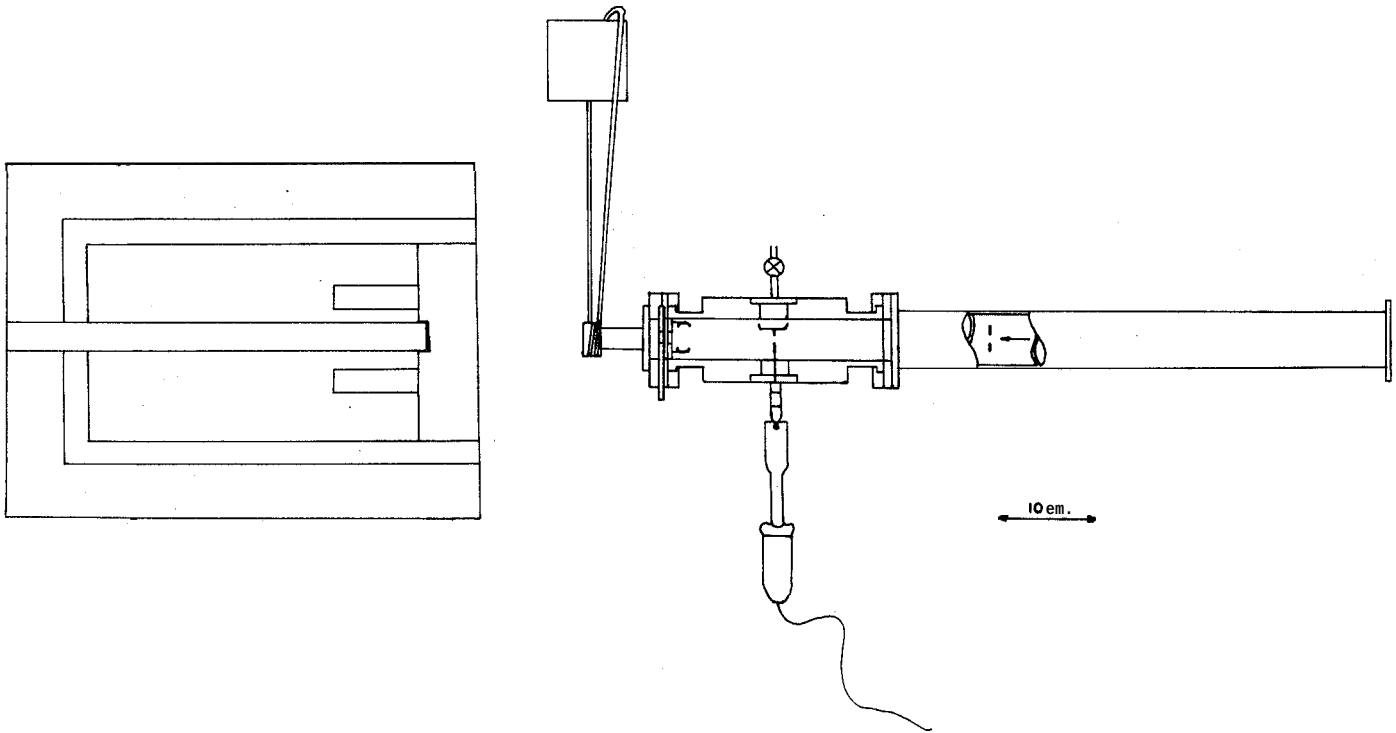

Fig. 3 - Modified scattering charnber and long counter geometry for the $D(^{16}O,n)^{17}F$ reactions. Heavy water (D_2O) is introduced through the valve and vaporizes on a copper surface heated by the soldering rod. It condenses on a copper surface cooled by a liquid nitrogen circulator.

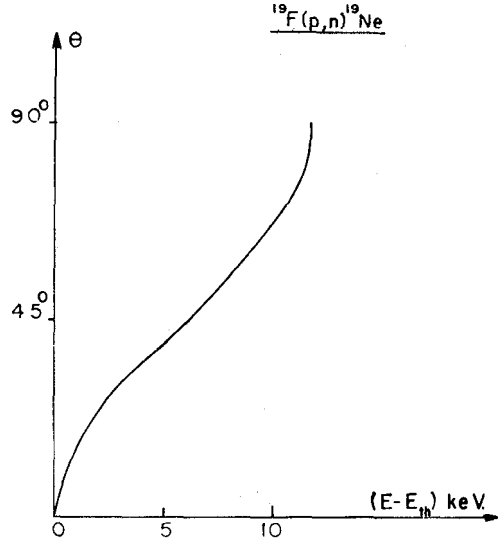

Fig.5 - Half angle opening of the neutron cone as a function of incident energy for the $^{19}F(p,n)^{19}Ne$ reaction.

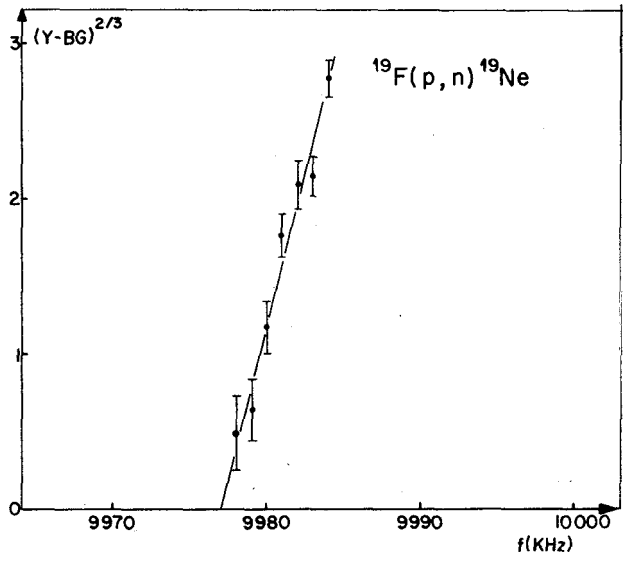

Fig.6 - Least squares fit to the experimental points as a function of NMR frequency (two-thirds power relation) for the $^{19}F(p,n)^{19}Ne$ reaction.

chamber to the turbo-molecular pump. All metallic parts are heated to avoid condensation, except the copper surface at left which is maintained at liquid nitrogen temperature. Ice layers of an estimated thickness of 1 mm were obtained by this procedure.

4. (ii) DETECTORS

Neutrons were detected with two standard BF_3 gas filled proportional counters. The counter ratio method[14] was used to locate the thresholds. However, due to the relatively low yield of fast neutrons, in (p,n) and (α,n) reactions, the fast neutron detector was used only as a monitor during the actual measurements. The slow neutron yields, after subtraction of the background contributions, were fitted to the two-thirds power law with the aid of a least squares fitting program to obtain the threshold frequencies. In the case of ^{16}O induced reactions, the slow neutron detector served the purpose of a monitor and the threshold frequencies were obtained from the fast detector data.

Figure 4 presents the top view of the slow counter. To enhance the sensitivity of this detector to the slow (keV) neutrons produced near threshold, the BF_3 counter was surrounded with a thin (1/2 inch) paraffin cylinder. This geometry, however, limits the energy range in which the two-thirds power law is applicable. Neutrons produced near threshold are contained in the interior of a cone of half-angle given by

$$\theta = \sin^{-1}\left(\frac{M_2 M_4}{M_1 M_3} \cdot \frac{E - E_{th}}{E} \right)^{1/2} . \qquad (3)$$

Figure 5 shows this angle, as a function of incident energy, for the $^{19}F(p,n)^{19}Ne$ reaction. The sensitive region was estimated to subtend a half angle of $\theta \simeq 40^0$ at the target, and Eq.3 determines that only experimental points, up to 5 keV above threshold, can be expected to obey the two-thirds power law. In the case of the $D(^{16}O,n)^{17}F$ reaction, due to the fact that the energy of the center of mass motion is large, expression 3 results in a slow opening of the cone as a function of inci-

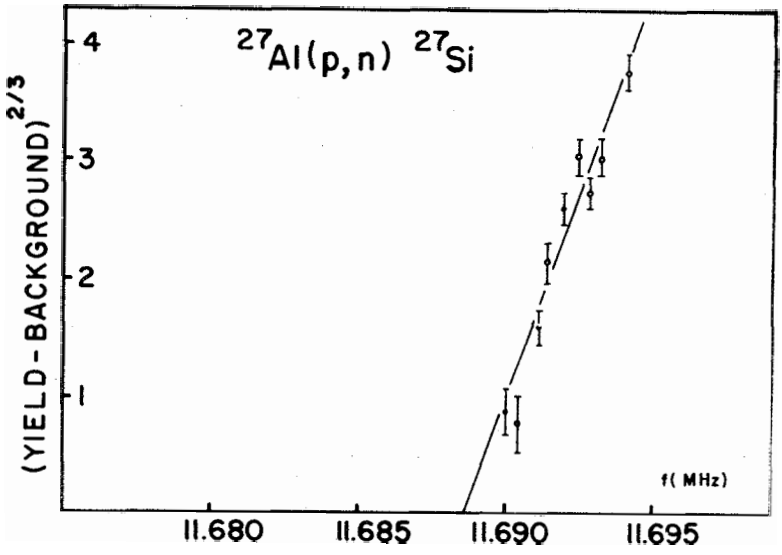

Fig.7 - The same as Fig. 6 for the $^{27}Al(p,n)^{27}Si$ reaction.

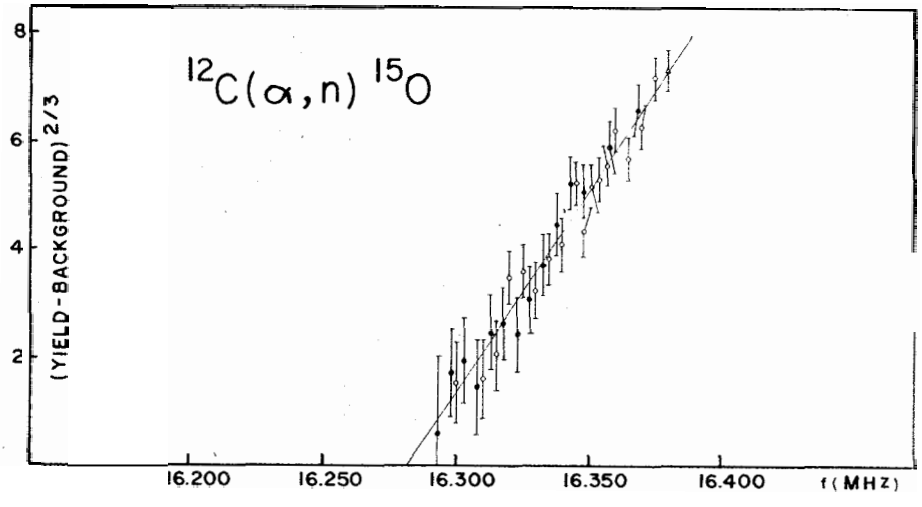

Fig.8 - The same as Fig. 6 for the $^{12}C(\alpha,n)^{15}O$ reaction.

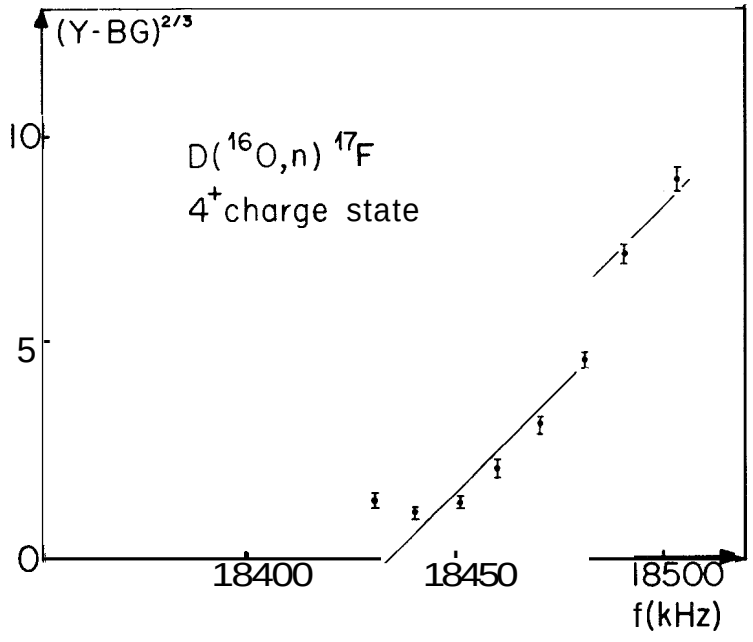

Fig.9 - The same as Fig. 6 for the $D(^{16}O^{4+},n)^{17}F$ reaction.

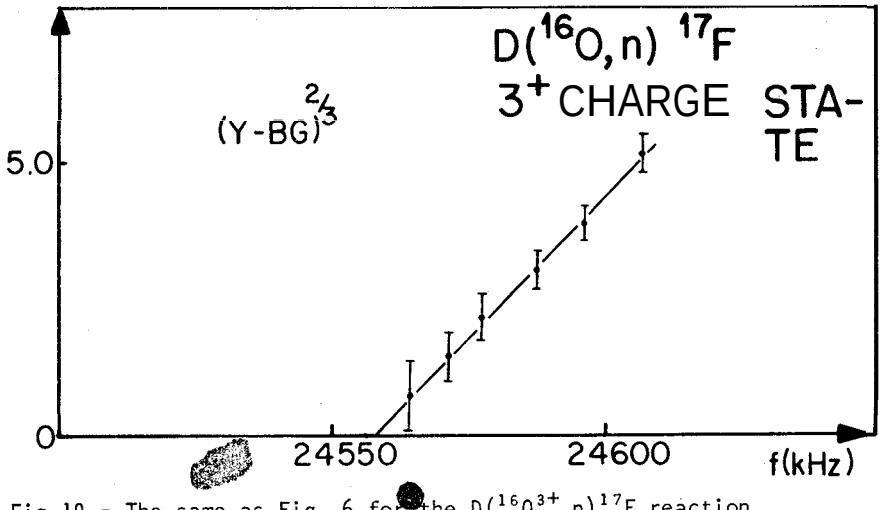

Fig.10 - The same as Fig. 6 for the $D(^{16}O^{3+},n)^{17}F$ reaction.

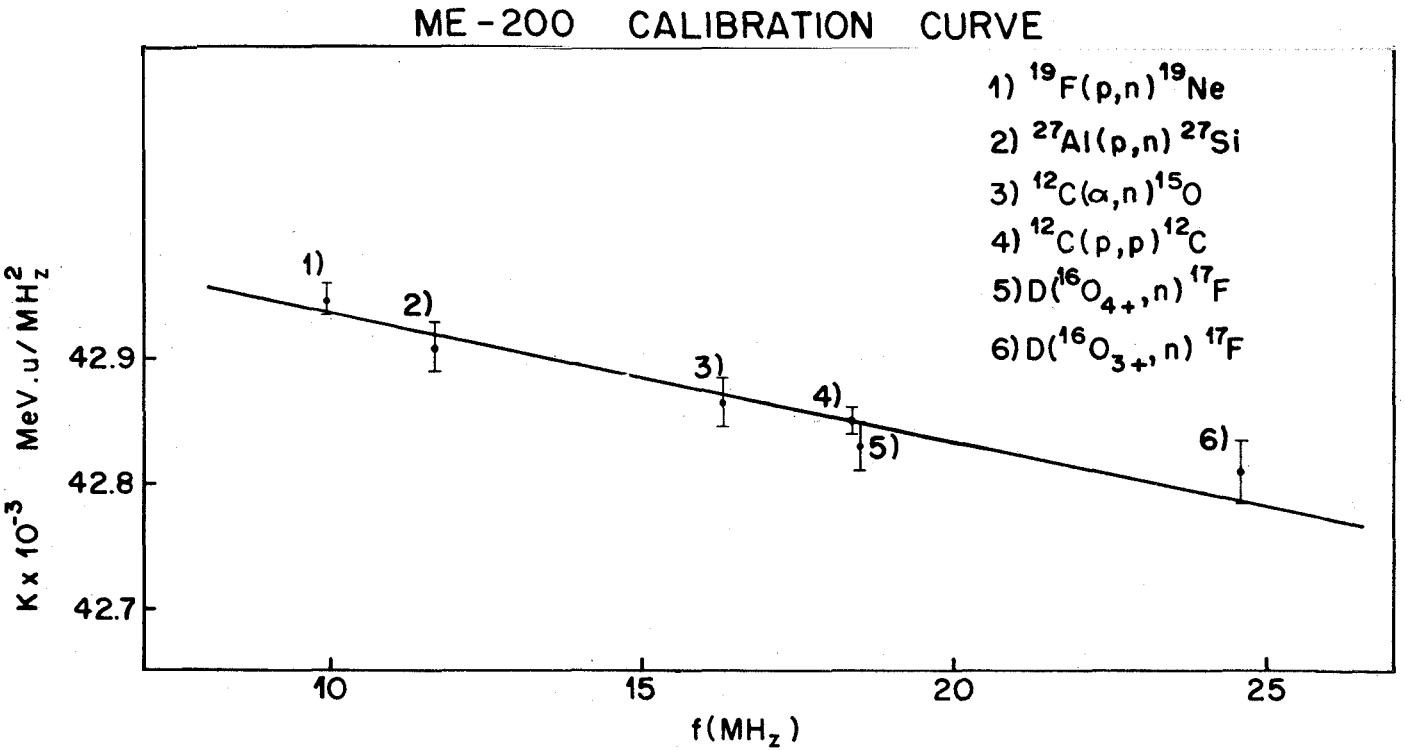

Fig.11 - Calibration constants as a function of NMR frequency at threshold for the calibration reactions. The straight line is a least squares fit to these points.

dent energy. At 100 keV above threshold, theopening is only 14^0 and the extrapolation range was not limited by the detector geometry.

5. RESULTS

Figures 6 to 10 show the least-squares fits to the experimental points on the 2/3 power plot. The threshold frequencies thus obtained and the energy standards are shown in Table 2 along with the calibration constants calculated from Eq. 2. Figure 11 shows the values of k as function of NMR frequency (proportional to the magnetic field), where the expected dependence of the calibration constant on the applied field is clearly observed.

This dependence may be explained as follows: as soon as current is supplied to the coils, the entrance and exit faces of the magnet begin to saturate due to the sharp field boundaries. As the current is increased, the saturated region extends inward and it is necessary to maintain a higher field in the center, to obtain the necessary average field along the particle trajectory for the particular energy. The NMR probe is positioned at the center of the beam trajectory, and therefore measures this higher field. This results in higher threshold frequencies and, as can be seen from Eq. 2, smaller calibration constants. The design of contoured pole edges[15], as in our magnet, has minimized but not completely eliminated this effect.

The dependence of k, on the NMR frequency, could be represented by the linear relationship.

$$k = (43.042 - 0.0104\, f) \times 10^{-3} \text{ MeV u/MHz}^2.$$

REFERENCES

1. Oscar Sala and G. Spalek, Nuclear Instruments and Methods 122, 213 (1974).
2. R. O. Bondelid, E. E. Dowling Whiting: Phys.Rev. 134-b, 591 (1964).

3. J. B. Marion: Revs.Mod. Phys. 38, 660 (1966).
4. E. H. Becknwer, R. L. Bramblett, G. C. Phillips and T. A. Eastwood , Phys. Rev. 123, 2100 (1961).
5. A. Rytz, H. Winkler, F. Zamboni and W. Zynch, Helv. Phys. Acta, 34, 819 (1961).
6. J. H. E. Mattauch, W. Thiele and A. H. Wapstra, Nucl.Phys. 67,1 (1965).
7. R. E. Shamu, E. M. Bernstein, D. Blondin and J. J. Ramirez Nucl. Phys. 189, 220 (1972).
8. B. E. Bonner, G. Rickards, D. L. Bernard, G. C. Phillips, Nucl.Phys. 86, 187 (1966).
9. J. M. Freeman, J. H. Montague, G. Murray, R. E. White and W.E. Burcham, Nucl. Phys. 65, 113 (1965).
10. J. C. Overley, P. D. Parker and D. A. Bromley, Nucl. Instr. & Methods 68, 61 (1969).
11. R. E. Shamu, E. M. Bernstein and M. J. Parrot, Nucl.Instr.& Methods 114, 605 (1974).
12. R. O. Bondelid, J. W. Butler and C. A. Kennedy, Phys. Rev. 120, 889 (1960).
13. A. H. Wapstra and N. B. Gove, Nucl. Data Tables 9, 267 (1971).
14. T. W. Bonner and C. F. Cook, Phys. Rev. 96, 122 (1954).
15. C. M. Braams, Nucl. Inst. & Methods 26, 83 (1964).
16. E. Huenges, H. Rosler, H. Jonach: Phys. Lett., 46-B, 361 (1973).

TABLE II

REACTION	ENERGY STANDARD (MeV ± keV)	REF.	TARGET	THRESHOLD FREQUENCY (MHz ± KHz)	MAGNET CONSTANT $\times 10^{-3}$ MeV.u/MHz^2
$^{19}F(p,n)^{19}Ne$	4.2343 ± .8	3	CaF_2	9.9768 ± 1.1	42.946 ± .012
$^{27}Al(p,n)^{27}Si$	5.8029 ± 3.8	9	99.9% pure Al	11.6896 ± 1.2	42.908 ± .03
$^{12}C(\alpha,n)^{15}O$	11.3408 ± .9	11	graphite	16.2815 ± 4.3	42.863 ± .023
$^{12}C(p,p)^{12}C$	14.23075 ± .20	16	carbon foil	18.359 ± 2.0§	42.851 ± .009
$D(^{16}O^{4+},n)^{17}F$	14.523 ± 5.	*	D_2O ICE	18.4144 ± 2.2	42.831 ± .018
$D(^{16}O^{3+},n)^{17}F$	14.5235 ± 5.	*	D_2O ICE	24.5591 ± 4.5	42.811 ± .022

* Calculated from $^{16}O(d,n)^{17}F$ threshold (Sec.3d)

§ J.H. Hirata - Thesis